Environ. Sci. Technol. **1998**, *32,* 2839−2845

Surface Oxidation of Pyrite as a Function of pH

PASCALE BONNISSEL-GISSINGER,† MARC ALNOT,† JEAN-JACQUES EHRHARDT,† AND PHILIPPE BEHRA*,‡

Laboratoire de Chimie Physique pour l'Environnement, UMR 7564 CNRS—Université Henri Poincaré, 405 rue de Vandœuvre, F 54600 Villers-lès-Nancy, France, and Institut de Mécanique des Fluides, UMR 7507 Université Louis Pasteur—CNRS, 2 rue Boussingault, F 67000 Strasbourg, France

Pyrite, the most abundant metal sulfide at the surface of Earth, plays a key role in many processes such as acid mine drainage, redox cycling of metals at oxic-anoxic boundaries of lake bottom, and degradation of pollutants. The oxidation of pyrite was studied in batch experiments over a large range of pH (2.5−12), with trace oxygen. Surface analysis of the samples was performed using X-ray photoelectron spectroscopy (XPS). Speciation of the aqueous species was investigated by inductively coupled plasma atomic emission spectrometry (ICP-AES), ionic chromatography, and UV−vis spectrophotometry. The pyrite surface can drastically change with the pH, which was never at steady state and tended to reach an acidic value whatever the initial pH. For pH <4, Fe(II) and SO_4^{2-} were released into solution; from XPS analyses, the pyrite surface presented O−H groups, an Fe-deficient composition $Fe_{1-x}S_2$, and iron(III) (hydr)oxide traces. Whatever the pH, the sulfur of the FeS_2 surface was mainly under the (−I) state oxidation. When the pH increased, Fe(II) disappeared and the surface was covered with iron(III) (hydr)oxides. This overlayer did not passivate the sample against further oxidation, and a decrease in pH was still observed.

Introduction

Pyrite (FeS_2) is the most abundant metal sulfide at the surface of Earth. This mineral is involved in many processes; some of them are of a crucial importance for environmental and geological concerns (*1*). The formation of acid mine drainage, the mobilization, precipitation, dissolution and redox cycling of metals in sediments, the degradation of pollutants, and the nutrient and metal cycling at oxic-anoxic boundaries of lake bottom and in estuaries are some of the domains in which the specific properties of pyrite are involved (*2*−*6*). Many of these properties are clearly related to the oxidative dissolution of pyrite. In natural aquatic systems, the important oxidants of pyrite are mainly oxygen and iron(III) (*2, 7*−*12*).

The overall reaction of pyrite with oxygen is usually expressed by reactions 1 and 2 in acidic media and by reaction 3 in basic conditions (*13*):

$$2FeS_2 + 7O_2 + 2H_2O \rightarrow 2Fe^{2+} + 4SO_4^{2-} + 4H^+ \quad (1)$$

$$2Fe^{2+} + {}^1/_2O_2 + 2H^+ \rightarrow 2Fe^{3+} + H_2O \quad (2)$$

$$2FeS_2 + {}^{15}/_2O_2 + 7H_2O \rightarrow 2Fe(OH)_{3(s)} + 4SO_4^{2-} + 8H^+ \quad (3)$$

The rate of reaction 2 is reported to be slow in acidic media (*2, 14*). The oxidation of pyrite by Fe^{3+} in acidic conditions is given by the following reaction:

$$FeS_2 + 14Fe^{3+} + 8H_2O \rightarrow 15Fe^{2+} + 2SO_4^{2-} + 16H^+ \quad (4)$$

The elementary processes at the atomic scale are not yet definitively established. Earlier studies are consistent with a pyrite oxidation mechanism whose rate-controlling step is a chemical reaction occurring after the initial adsorption of oxygen to the pyrite surface (*9*). More recent papers have pointed out interfacial electron transfer with formation of thiosulfate as key parameter for the oxidation (*10, 11*). However, it appears that pyrite oxidation in aqueous medium is a much more complex mechanism depending on many factors (*12*). Indeed the concentration of dissolved oxygen, the specific area, the grinding or polishing conditions, the presence of impurities, the concentration of ferric ions in solution, the temperature, and the presence of bacteria (*12, 13*) could drastically influence the oxidation rate. It is worth noting that depending on their source, some pyrites could present at their surface a quite large enrichment in polysulfides, whereas the surface of some other samples is almost free of sulfur (*15*). This large diversity of behavior is certainly at the origin of some of the discrepancies found in the literature when looking at the surface characterization of pyrite. A lot of methods such as electrochemistry (*16*), X-ray photoelectron spectroscopy (XPS) (*17, 18*), infrared and Raman spectroscopies (*19, 20*), electrophoretic mobility measurements (*21, 22*), and scanning tunneling microscopy (*6*) have been used. Many questions are still the subject of debate. Formation of elemental sulfur or polysulfides and the nature of intermediate and final products of oxidation are some of the questions which stimulate new experiments (*18*−*20*).

Our primary interest in pyrite surface chemistry was the investigation of the mechanisms of sorption of metals as a function of pH. For example, it has been established that mercury presents a very high affinity toward sulfides, the usual interpretation being the formation of HgS which has a very low solubility product (*23, 24*). Our basic idea was to have a deeper insight into the origin of the surface reactivity of pyrite in aqueous solution, the nature of the active sites for sorption processes being unclear. It is often believed that the reactivity of pyrite is governed by S−S−H groups at least in anoxic conditions. It would be tempting and useful to develop a surface complexation model for sulfides based on the reactivity of S−S−H groups, as it has been previously established for O−H groups at the surface of (hydr)oxides (*25, 26*). However, in the presence of dissolved oxygen, it could be postulated that either S−S−H or O−H groups play a role. Furthermore, as a consequence of the oxidative dissolution of pyrite, iron-deficient sulfide species have sometimes been observed at the surface (*18, 27*), giving rise to other possibilities for active sites such as iron vacancies. Finally, the literature cited above shows that the surface reactivity of pyrite strongly depends on the experimental conditions such as the pH and/or the contact time. A careful

* Corresponding author telephone: 33 (0) 388 416 563/565; fax: 33 (0) 388 614 300; e-mail: behra@imf.u-strasbg.fr.
† Laboratoire de Chimie Physique pour l'Environnement.
‡ Institut de Mécanique des Fluides.

S0013-936X(98)00213-2 CCC: $15.00
Published on Web 08/29/1998

TABLE 1. Composition of Pyrite Impurities (wt %)

impurity	SiO_2	Al_2O_3	MnO	MgO	CaO	Na_2O	K_2O	TiO_2	P_2O_5	Cu	Pb	Zn
%	1.17	0.41	0.02	0.16	0.23	<0.01	0.05	0.12	0.07	0.13	0.13	0.08

characterization of the surface is a necessary prerequisite prior to attempting any modeling for sorption of pollutants. In this paper, the surface properties of pyrite will be spectroscopically investigated in terms of (i) surface stoichiometry compared to the bulk, (ii) nature of active sites, and (iii) nature of the surface chemical compounds formed during the interactions with the solution. In parallel, changes in the composition of the solution will also be studied as a function of the contact time to test if steady-state conditions can be reached.

Experimental Methods

Mineral Preparation. The pyrite used in our experiments came from a Peruvian mine. Its chemical analysis gave a stoichiometric ratio Fe/S of 0.505. The pyrite which contained around 3% of impurities, especially silica (Table 1), was characterized by X-ray diffraction and Mössbauer spectroscopy. The spectra were consistent with the reference standards. Pyrite was used as plates or powders. Pyrite plates were prepared by cutting 1 × 1 cm^2 sections. They were then polished and rinsed with ethanol and 10^{-2} M nitric acid to eliminate oxidation products. Powders were prepared by grinding in an agate mortar. The powder was sieved between 40 and 80 μm except for electrophoretic mobility measurements (1 and 10 μm to avoid sedimentation). The oxidation products were eliminated by rinsing with 10^{-2} M HNO_3. Pyrite was then stored under vacuum, until use. The specific surface area of the crushed powder was estimated to be 0.4 $m^2\ g^{-1}$ (Kr BET at 77 K).

After dry grinding in the agate mortar, oxidation products appeared at the FeS_2 surface (Figure 1). The XPS analyses showed that sulfates and iron(III) (hydr)oxides were present at the surface. Even prepared under inert conditions (grinding in a glovebox under N_2), the pyrite surface was oxidized: 20% of the total sulfur and 32% of the total iron present in surface. The estimation was made according to the decomposition of the spectra as explained in the part concerning XPS. After washing with HNO_3, the oxidation products were released into solution and at the FeS_2 surface, sulfates disappeared whereas a small peak of iron(III) (hydr)-oxides still remained at 711.7 eV.

Pyrite Oxidation. For all experiments, chemicals were of analytical grade. Water used for solution preparation was Milli-Q degassed water (Millipore). Ionic strength was fixed with $NaNO_3$ (Merck, p.a.). Pyrite contact time was 36 h with the exception of the experiments in which kinetics was studied. Experiments were performed in 40 mL Teflon centrifuge tubes at 25 °C. The initial pH was adjusted with nitric acid (Merck, p.a.) or decarbonated sodium hydroxide (J. T. Baker, p.a.). It was not corrected during the experiments. Separation of phases was done by centrifugation of the tubes at 25 °C with an acceleration of 28000*g*. The pH of the supernatant was then measured.

Solution Analyses. The pH was monitored using an Orion Ross combined glass electrode (no. 8102) filled with 3 M KCl. The electrode was calibrated with standard buffer solutions (pH 4 and 7 or 9 and 7). Total dissolved iron and sulfur species were analyzed by ICP-AES using a Perkin-Elmer Emission Spectrometer 2000 (detection limits 2.70 and 30 μM for total iron and sulfur, respectively). Iron speciation was studied with a Beckman DU 7500 UV−vis spectrophotometer. Aqueous total iron(II) and iron(III) were, respectively, determined by the orthophenantroline method at 507 nm and thiocyanate method at 480 nm with a detection limit of 1 μM. Standards were prepared with $FeSO_4 \cdot 7H_2O$ (Prolabo, p.a.). Sulfur speciation was studied by ion chromatography (Waters 501) equipped with a conductometric detector Waters model 430 and a UV detector Waters 486. The anion-exchange column of 50 mm length (Waters 07355) contained a porous polymethacrylate gel with a quaternary ammonium function group; the eluent was a borate glucanate buffer of pH 8.2. The UV detection was done at 220 nm. Standards were prepared with $Na_2S_2O_3 \cdot 5H_2O$ (Fluka, p.a.), with Na_2SO_3 (Fluka, p.a.), and with a standard anion multielement solution (Cl^-, NO_3^-, SO_4^{2-} at 1 g L^{-1}, Merck). The detection limits were 30 μM for SO_4^{2-}, $S_2O_3^{2-}$ and SO_3^{2-}.

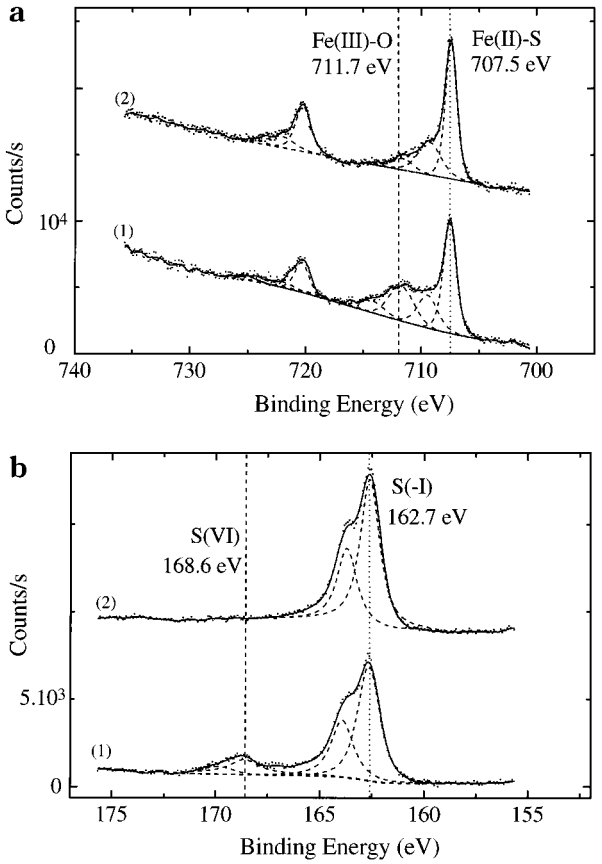

FIGURE 1. Comparison of XPS spectra of pyrite for (a) Fe 2p, (b) S 2p, after grinding (1), or both grinding and washing with HNO_3 (2).

Electrophoretic Mobility Measurements. Electrophoretic measurements were performed with a Sephy 33-MDV-944 apparatus. Cu electrodes were covered with a 20 μm Pd thin film electrolytically deposited. Pyrite suspensions (1−10 μm) were prepared with Milli-Q water. Suspensions of 2 g L^{-1} were stirred during 36 h. Ionic strength was fixed with 1 mM $NaNO_3$ and pH with HNO_3 or NaOH; pH was measured before and after each electrophoretic measurement. A potential between 50 and 100 V was applied to each suspension. The average electrophoretic mobility was converted to ζ-potential using the Henry's equation.

X-ray Photoelectron Spectroscopy (XPS). The X-ray photoelectron spectrometer was extensively described in a previous paper (*28*). Briefly, the XPS spectra were obtained using unmonochromatized MgKα (1253.6 eV) source of photons, the pressure in the analytical chamber being in the low 10^{-7} Pa range. The spectrometer work function was

TABLE 2. XPS-Binding Energies for Relevant Chemical Species Reported in the Literature

species	binding energy (eV)	source
	Fe($2p_{3/2}$)	
Fe(II)-S	707.0	Mycroft et al. (*20*)
	707.4	Karthe et al. (*18*)
	707.0	Nesbitt and Muir (*37*)
	707.45	Pratt et al. (*32*)
	707.1	Eggleston et al. (*6*)
surface defects	709.2	Pratt et al. (*32*)
	708.75	Nesbitt and Muir (*37*)
	709.85	Nesbitt and Muir (*37*)
FeO	709.6	Mills and Sullivan (*38*)
Fe_3O_4	710.8	Mills and Sullivan (*38*)
α-Fe_2O_3	711.0	Harvey and Linton (*39*)
	711.0	Ferris et al. (*40*)
α-FeOOH	711.9	Ferris et al. (*40*)
	712.1	Scheidegger et al. (*41*)
	S($2p_{3/2}$)	
S^{2-}	161.1	Buckley and Woods (*27*)
	161.3	Pratt et al. (*32*)
S_2^{2-}	162.4	Van der Heide et al. (*42*)
	162.5	Mycroft et al. (*20*)
	162.45	Eggleston et al. (*6*)
S_n^{2-}	165.3	Wagner et al. (*43*)
S_8	164.2	Carlson *(31)*
	163.8	Wagner et al. (*43*)
	163.7	Hyland and Bancroft (*44*)
SO_4^{2-}	169.1	Wagner et al. (*43*)
	168.5	Jones et al. (*45*)
	O(1s)	
α-FeOOH		
oxide	530.0	Ferris et al. (*40*)
	530.1	Scheidegger et al. (*41*)
hydroxide	530.9	Harvey and Linton (*39*)
	532.1	Scheidegger et al. (*41*)
physically adsorbed H_2O	532.3	Harvey and Linton (*39*)
	533.8	Jones et al. (*45*)

adjusted to give a value of 84.0 ± 0.05 eV for the Au $4f_{7/2}$ level of metallic gold. The survey scans were recorded using a fixed pass energy of 90 eV, while narrow scan spectra of the S 2p, Fe 2p, and O 1s levels were recorded using a fixed pass energy of 22 eV. As charge effects were expected in the study of these poorly conducting samples, the binding energy of the C 1s level from contamination at 284.6 ± 0.1 eV was used as internal reference to calibrate every spectrum. Scofield (*29*)-calculated cross-sections and the inelastic mean free path (*30*) were used for quantification. Selected values of reference binding energies are given in Table 2. The recorded lines were fitted using a curve-fitting program with Gaussian Lorentzian or asymmetric peak shapes, respectively, for S 2p and O 1s and for Fe 2p. The S 2p peaks were fitted using doublets $2p_{1/2}$, $2p_{3/2}$ of 1.4 eV in width (fwhm), separated by a spin−orbit splitting of 1.1 eV. The S ($2p_{1/2}$) peak area was constrained to one-half of the area of the S ($2p_{3/2}$) peak. The O 1s peak was decomposed into three components at 530.4 ± 0.1 eV, 531.8 ± 0.1 eV, and energies higher than 533 eV associated, respectively, with O^{2-} ions of the oxides, OH^- of the hydroxides, and molecular water sorbed onto the surface of the samples. Fe 2p levels were fitted taking into account the various contributions of iron(II) and iron(III) compounds. Ferrous sulfide contribution of pyrite was limited to a narrow primary peak at 707.5 eV, in agreement with the single possible final state $2p^53d^6$. The tail at the high binding energy side which was always observed on pyrite was fitted with a component at 709.5 eV certainly associated with a ferrous (hydr)oxide contribution (see Table 2). Ferric oxygen compounds were characterized by a main peak at 711.6 ± 0.2 eV associated with two other broad peaks at 714.3 ± 0.2 and 717.0 ± 0.2 eV which were introduced to include the multiplet splitting (five final states for the photoemission of the 2p level of an initial configuration of $3d^54s^0$ of Fe^{3+}) and the possible satellite structures (*31*). The fitting procedure was a simplified version of the procedure described by Pratt et al. (*32*).

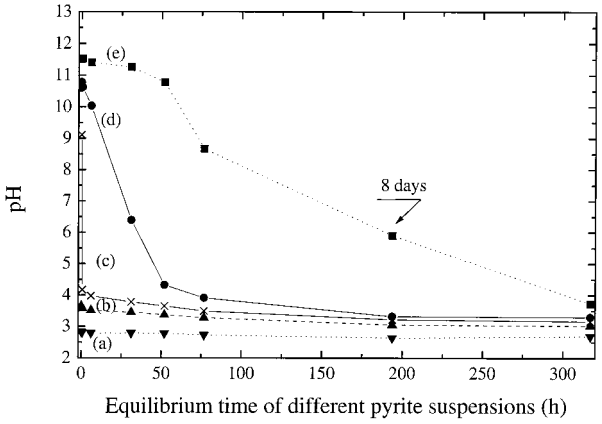

FIGURE 2. Variation of pH of an FeS_2 suspension (2 g L^{-1}) vs time in batch reactors for different initial pH. I = 10 mM ($NaNO_3$).

Experimental Results

Oxidation Kinetics as a Function of pH. Kinetic experiments were performed between 0 and 13 days. Although experiments were conducted in batch reactors, the pH of the pyrite suspensions were not stable (Figure 2). In acidic pH range (2−4), pH slowly decreased vs time. When pH was neutral or basic (7−10), it rapidly decreased to a value close to 4 (within 36 h). For pH higher than 11, the kinetics was much slower; after 36 h, the pH was still basic. Whatever the initial pH, the studied systems tended to reach a more acidic pH. These results suggest the presence of dissolved oxygen in solution, which could induce pyrite oxidation and in turn liberation into solution of chemical species, such as protons. A possible source of oxygen could be gas diffusion through Teflon tube walls.

Aqueous Fe and S Speciation. In the pH range between 2 and 4.5, pyrite was oxidized into Fe(II) and SO_4^{2-} (Figure 3). Neither iron(III) nor S species were detected with the analytical techniques used. The pH did not influence the Fe(II) and the amount of free sulfate in this pH range; almost two SO_4^{2-} ions are released for one Fe(II) ion. The molar ratio Fe(II)/SO_4^{2-} is equal to 0.5 ± 0.1.

When the pH was higher than 4.5, our analytical techniques did not allow detection of Fe in solution. As observed by Goldhaber and Moses et al. (*7*, *9*), the aqueous S speciation was changed; in addition to sulfate, thiosulfate appeared in the solution at neutral pH, and both thiosulfate and sulfite were present at basic pH. The higher the pH, the higher the concentration of sulfur compounds in solution.

The influence of nitrate ions as a possible oxidant of pyrite was also studied. Experiments were performed for suspensions of FeS_2 with $NaNO_3$, with NaCl, and without salts. The concentrations of Fe and S released in solution were the same in the three cases at low pH. Therefore, the nitrate ions were not responsible for the oxidation of pyrite.

Surface Analyses by XPS. Fe 2p, S 2p, and O 1s spectra recorded after putting the pyrite in contact with a solution at various initial pH values are reported in Figure 4. These spectra were decomposed according to the procedure presented in the previous section.

Fe $2p_{3/2}$ Spectra. In the acidic range (pH <4), Fe ($2p_{3/2}$) spectra (Figure 4a) were dominated by the characteristic peak of pyrite at 707.5 ± 0.2 eV in agreement with previously

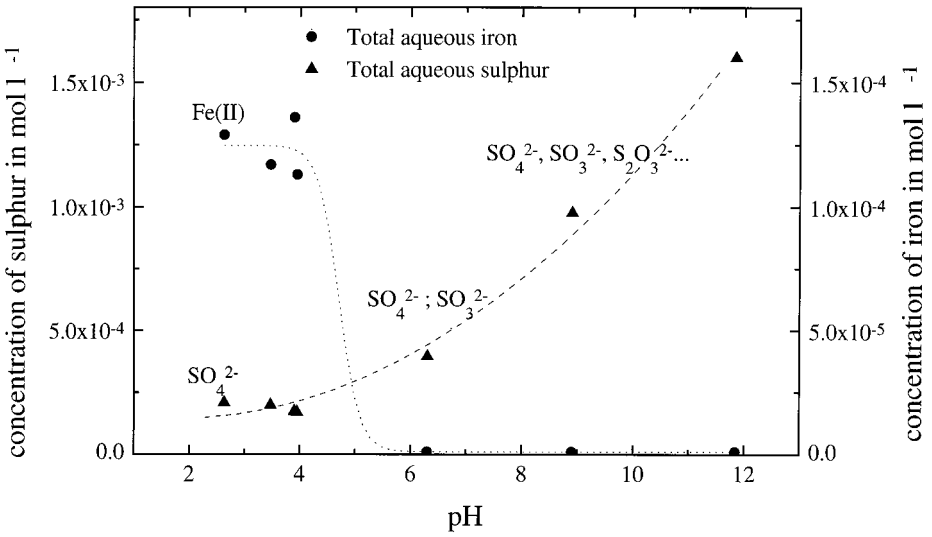

FIGURE 3. Aqueous speciation of Fe and S released from pyrite vs pH. Experimental conditions: FeS_2 suspensions = 2 g L^{-1}, I = 10 mM ($NaNO_3$), reaction time = 36 h.

published values (*18*). The high binding energy tail was fitted with three wide peaks (fwhm around 2−3 eV) at 709.4 ± 0.2, 711.6 ± 0.2, and 714.3 ± 0.2 eV. The feature at 709.4 eV is not usual. It could be due either to the defects introduced by grinding or polishing or to energy-loss processes due to inelastic scattering and multielectron excitations which can induce a satellite peak or to some ferrous (hydr)oxide traces at the surface of the samples. A contribution at 708.8 eV has been reported on fractured and scraped samples by Karthe et al. (*18*) and assigned to an FeS-like emission. In our study, the dissolution process could have suppressed most of these surface defects. Moreover, no clear evidence of a S^{2-} contribution is observed in the S 2p spectra (Figure 4b). So we believe that the peak at 709.4 eV indicates the presence of some surface ferrous (hydr)oxides as attested by the presence of a OH^- component in the O 1s spectra (Figure 4c). But some surface defects which contribute to this peak cannot be excluded. The peak at 711.6 eV in the Fe ($2p_{3/2}$) spectra is attributed to iron(III) (hydr)oxides. Finally the intensity of the peak at approximately 714.3 eV, which is due to an iron(III) multiplet structure, is very low.

As the pH increased, the peak at 711.6 eV associated with the iron(III) (hydr)oxides strongly increased in the Fe ($2p_{3/2}$) spectra. Conversely, the peak for pyritic Fe at 707.5 eV decreased, indicating that the surface was progressively covered with a thick layer of oxide. Finally, in the basic pH range, Fe(II) completely disappeared, indicating that the thickness of the overlayer was larger than 3 nm (assuming an escape depth of about 1.5 nm).

S 2p Spectra. S(2p) spectra are reported in Figure 4b as a function of the initial pH of the aqueous-contacting solution. Whatever the pH, no significant difference concerning S peak shapes was observed. The binding energy of the S $2p_{3/2}$ is centered at 162.7 ± 0.1 eV in agreement with the expected value for pyritic S(−I) S_2^{2-} (see Table 2). All the spectra have been reasonably fitted with a single doublet, which evidences a single S oxidation state on these samples. However, as the detection of elemental S or polysulfide (S_n^{2-}, $n > 2$) compounds was difficult by XPS because of their volatility in the low vacuum of the XPS analytical chamber, an experiment was performed with the sample cooled at −180 °C before introducing it into vacuum. A small S_8 shoulder can be observed at low pH. At higher pH, the absence of any significant signal in the range 164−165 eV ruled out the presence of elemental S or S_n^{2-} at the surface in our conditions. Moreover, within the detection limits, no traces of sulfates or sulfites were found in the 166−169 eV range. In conclusion, S was primarily present at the pyrite surface under (−I) state oxidation, whatever the pH.

O 1s Spectra. The O 1s spectra are shown in Figure 4c. Decomposition into three peaks associated with oxide, hydroxide, and molecular water was sufficient to fit O 1s spectra in most of the cases. However, for experiments corresponding to a final pH of 4.5 with an initial pH of 4.5 or 9.0, extra peaks were observed at 535 ± 0.1 eV and/or 537.6 ± 0.1 eV. These extra peaks may reveal an island growth mechanism of the iron (hydr)oxides at the surface of pyrite. Indeed, the analysis of Fe 2p and of O 1s levels clearly indicates the presence of these two compounds at pH 4.5. Analysis of rough spectra before charge effect correction by adventitious carbon does not show any charge effect. This could actually be a double charge effect due to the fact that pyrite has semiconductive properties, whereas iron (hydr)oxides behave as insulating materials. In the high pH range, it is worth noting the O 1s peak is properly fitted with the components of oxide and hydroxide of almost equal intensity as expected in FeOOH (Table 3).

Surface Stoichiometry. Whatever the initial treatment of pyrite samples (grinding, polishing, cleaving, and reaction time in acid solutions), the Fe/S ratio calculated from XPS spectra was always between 0.28 and 0.31 (Table 3). So the pyrite surface did not exhibit the expected stoichiometry Fe(II)/S = 0.5. To check if this ratio was not due to an error in the values of the cross-section or the inelastic free path used for quantifying, a crystal of pyrite was directly polished in the analytical chamber of XPS spectrometer. The stoichiometry found in this experiment confirms the excess of sulfur with respect to Fe for FeS_2 samples treated outside the chamber. Sulfur present at the FeS_2 surface is mainly in the (−I) state oxidation. As mentioned above, no traces of S(−II), elemental sulfur, or polysulfides were detected by XPS, even at −180 °C, experimental conditions which should have favored the characterization of such species. Therefore, some defects at the pyrite surface could be due to the formation of vacancies as proposed by Karthe et al. (*18*):

$$FeS_2 \rightarrow Fe_{1-x}S_2 + xFe^{2+} \qquad (5)$$

The fingerprint of these defects could be to some extent found in the peak at 709.4 eV in the Fe $2p_{3/2}$ levels (see above).

Electrophoretic Mobility. The isoelectric point (iep) of pyrite samples was observed in the pH range 7−8 in our experimental conditions (Figure 5). Fornasiero et al. (*21*)

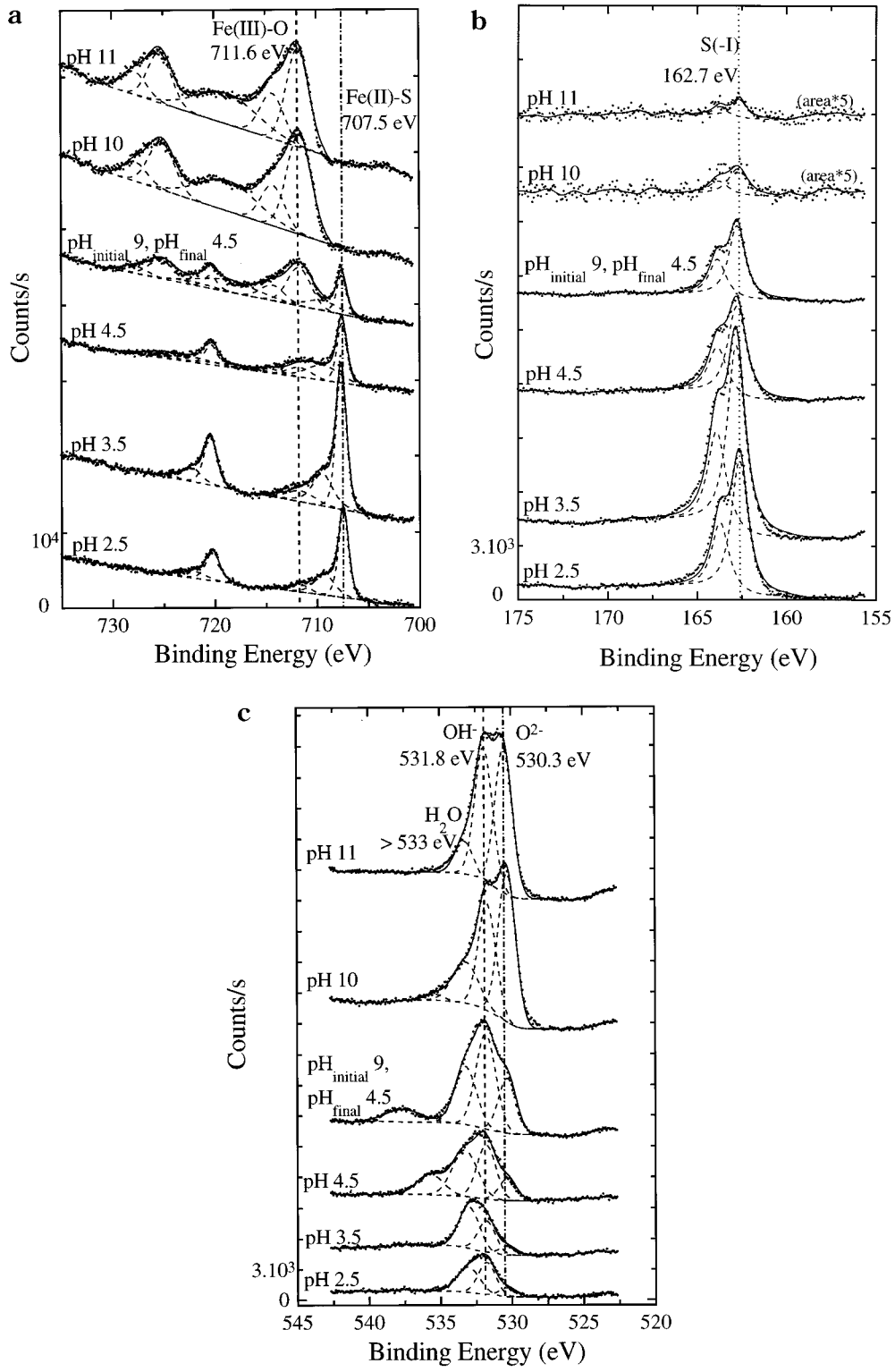

FIGURE 4. FeS_2 plates XPS (MgKα) spectra of (a) Fe 2p, (b) S 2p, and (c) O 1s in MgKα. Experimental conditions: I = 10 mM ($NaNO_3$), reaction time = 36 h. Initial pH values are indicated for each spectrum. Final pH is only indicated when different from initial pH (see Figure 2).

and, more recently, Bebie et al. (*22*) reported on the one hand an iep of 1.5 for a nonoxidized pyrite, which was ground, conditioned in water under N_2, and kept under inert N_2 atmosphere, and on the other hand, an iep higher than 6 for a pyrite sample kept under air. In the presence of air, the iep is close to the usual values of pH_{iep} reported for iron(III) (hydr)oxides such as goethite, lepidocrocite, and ferrihydrite, which lie between 6 and 9 (*33*). However, in both cases (*21, 22*), the composition of the surface was not checked by direct analyses, and the presence of sulfurs or polysulfides, which could lead to negatively charged surfaces down to very low pH, cannot be completely ruled out. In our conditions, no S compound other than pyritic S was detected, and Fe 2p and O 1s signals are evidence of the presence of iron(II) and iron(III) oxides and hydroxides. So, the oxidized compounds were certainly at the origin of the electrophoretic mobility behavior of pyrite we observed, and both observations are consistent.

TABLE 3. Comparison of Fe(II) and Fe(III) at the Pyrite Surface vs pH Estimated with XPS Spectrum Decomposition[a]

final pH	O^{2-}/OH^-	Fe(II)/S(−I)	$Fe(III)/(OH^- + O^{2-})$
pH 2.5	0.28	0.28	0.10
pH 3.5	0.28	0.30	0.12
pH 4.5	0.38	0.31	0.17
pH 4.5 ($pH_i = 9$)[b]	0.53	0.28	0.32
pH 10	1.36	ne[c]	0.54
pH 11	1.08	ne	0.50

[a] The reported ratios are calculated from the surface molar concentrations. [b] Initial pH (see Figure 2). [c] ne, not estimated (see Figure 4a).

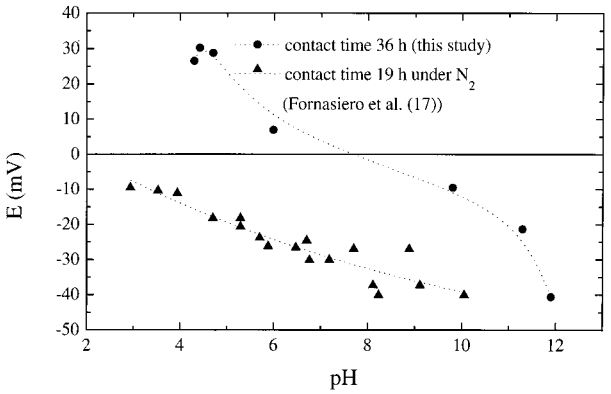

FIGURE 5. Electrophoretic mobility measurements of a pyrite suspension. Experimental conditions: FeS_2 suspension = 2 g L^{-1}, I = 1 mM ($NaNO_3$), contact time before measurements = 36 h. For comparison, experimental data of Fornasiero et al. (*21*) are reported too (FeS_2 suspension = 1.2 g L^{-1}, conditioning pH 5, I = 5 mM (KNO_3), contact time before measurements = 19 h under N_2 atmosphere).

Discussion

With both the analyses of the surface of FeS_2 and the released species into aqueous solution, we can have a better insight of the surface composition and reactivity of pyrite as a function of pH in the presence of a low amount of dissolved oxygen.

Domain of Acidic pH (2−4). Dissolved oxygen probably plays an important role in the pyrite oxidation since one Fe(II) ion is released into the aqueous solution for two SO_4^{2-} ions at low pH (<4) (Figure 3), which is roughly consistent with the oxidation reaction 1. The reaction of Fe^{2+} with NO_3^- could occur, but is much slower than with O_2 which explains the conservative behavior of NO_3^-. Iron(II) and iron(III) (hydr)oxides represent approximatively 15% of Fe present at the FeS_2 surface as calculated from XPS spectra (Figure 4). In a very crude layer by layer model, these compounds could constitute a fraction of a monolayer. This observation is evidence of the fact that, at pH <4.5, Fe^{2+} is more likely oxidized on the surface than in solution (*26, 34*). The presence of iron(III) species was further confirmed by electrophoretic mobility measurements which are consistent with the presence on the surface of positively charged species such as Fe^{3+}, $FeOH^{2+}$, and $Fe(OH)_2^+$ (Figure 5). Actually, we believe that these species are of crucial importance in the oxidation mechanism of pyrite, Fe^{3+} acting as a catalytic oxidant of this mineral. This is in agreement with the mechanism previously proposed first by Singer and Stumm (*2*) and recently extended by Moses and Herman (*8*). In this mechanism, adsorbed Fe species are cyclically oxidized and reduced and are considered as a preferential pathway for electrons travelling from FeS_2 to dissolved O_2, which is the ultimate oxidant. As a matter of fact, there is no XPS or other data supporting O_2 sorption onto the pyrite surface. Therefore, one of the main contribution of this study is a spectroscopic evidence of the presence of these catalytic centers on the surface.

From the point of view of cation sorption onto pyrite, it has to be noticed that even at low pH the surface of pyrite is very complex; Fe vacancies and surface groups such as O−H from coated iron(III) (hydr)oxides and S−S−H from pyrite can be considered as potential adsorption sites.

Domain of Neutral pH (4−10). In this pH range, the iron(II) oxidation to iron(III) in the aqueous phase is much faster (*3*) and the precipitation as iron(III) (hydr)oxides is more likely to occur. The pyrite surface appears, therefore, more heterogeneous and composed of both the Fe(II) of pyrite and the iron(III) (hydr)oxides (Figure 4, panels a and c). The higher the pH, the more iron (hydr)oxide at the FeS_2 surface. The $Fe(2p_{3/2})$ peak at 711.7 eV increases such as the O (1s) peaks at 530.4 and 531.8 eV. If we consider that water molecules can be sorbed onto either pyrite or iron (hydr)-oxides, it can be understood that two different binding sites of O 1s are expected, depending on the nature of the sorption sites of water. In other words, water molecules can be considered as a local probe of the conducting properties of the surface. This behavior, which we have observed many times, is circumstantial evidence of an island growth mechanism of iron(III) (hydr)oxides onto pyrite (Figure 4c).

However, the pyrite surface is not passivated since Fe(II), sulfates, and protons are still released into the aqueous solution, the measured concentrations strongly depending on the initial pH (between 5 and 10), which rapidly decreases till pH 4. In this domain of pH, the pyrite surface is very reactive and unstable due to its greater oxidation capability, which can be attributed to the presence of iron(III) as previously discussed.

Domain of pH >10. The pyrite surface oxidation rate increases at basic pH, and larger concentrations of sulfur species are released into solution. Iron(II) oxidation to iron-(III) is much faster at high pH. When the pH is higher, iron (hydr)oxides grow at the surface and more or less cover the pyrite surface. The S 2p spectrum area largely decreases as the pH increases. On the other hand, the oxide peak of O 1s spectra increases compared to the hydroxide peak. The $Fe(III)/(O^2 + OH^-)$ and O^{2-}/OH^- ratios reach approximately 0.5 and 1, respectively (Table 3). Iron (hydr)oxides formed at the pyrite surface present a stoichiometry close to FeOOH. Unfortunately, no characterization of these (hydr)oxides was possible by techniques such as Mössbauer or Raman spectroscopy because of lack of sufficient material.

The iron(III) (hydr)oxide coating does not prevent further FeS_2 oxidation because sulfur species and protons are still released to solution. If we suppose that this layer is homogeneous on the FeS_2 surface, the FeOOH thickness is about 5 nm at pH 10 and 6 nm at pH 11. This change in the surface composition is also consistent with specific surface area measurements (Kr BET, 77 K) done with ground pyrite, treated at different pH, and then dried. After the treatment at pH 3, the specific surface area of FeS_2 is equal to 0.4 m^2 g^{-1}, which is the value obtained for the crushed powder before treatment, whereas for the treatment at pH 11, it reaches 0.8 m^2 g^{-1}. The iron(III) (hydr)oxides at the surface would develop important specific areas (*35, 36*) which would modify those of FeS_2 (Figure 5). The reactivity of the pyrite in this pH domain would be expected to be close to iron(III) (hydr)-oxides with high affinity for cations.

Thanks to the analysis of both pyrite surface and solution which was in contact with the solid, we can have a rather good picture of the solid−water interface behavior. The pyrite surface can drastically change with the pH. Actually the pH of pyrite suspensions is never at steady state and tends to reach an acidic value (pH <4) whatever the initial pH probably due to the presence of low concentration of oxygen. These

experiments exemplify the acidic pH of drainage waters in mines and the possible consequences on the environment and groundwaters around them. In the acidic pH range, the pyrite surface presents a deficiency in iron which can be explained by formation of iron vacancies $Fe_{1-x}S_2$. When the pH increases, the surface is covered with iron(III) (hydr)-oxides with a stoichiometry close to FeOOH. Hydroxyl O−H and S−S−H surface groups coexist at the pyrite surface over the entire pH range. S−S−H groups are predominant in acidic conditions, while O−H groups are predominant at basic pH. Both groups are thus probably involved in the sorption of heavy metals by surface complexation surface mechanisms. The next step will be to improve our knowledge of the cation sorption by looking at the surface in the different explored domains of pH from the point of view of surface characterization of both pyrite and sorbed cations by spectroscopic techniques.

Acknowledgments

C. Louis, J. Cortot, J. Menaucourt, M. Abdelmoula, and J. Lambert are acknowledged for their assistance for ionic chromatography analyses, ICP-AES analyses, N_2 BET measurements, XRD and Mössbauer spectra, and XPS spectra, respectively. P.B.-G. was supported by a grant from CNRS and Région Lorraine. We also thank the three anonymous reviewers for helpful suggestions.

Literature Cited

(1) Morse, J. W.; Millero, F. J.; Cornwell, J. C.; Rickard, D. *Earth-Sci. Rev.* **1987**, *24*, 1.
(2) Singer, P. C.; Stumm, W. *Science* **1970**, *167*, 1121.
(3) Stumm, W.; Morgan, J. J. *Aquatic Chemistry*, 3rd ed.; John Wiley & Sons: New York, 1996.
(4) Lalvani, S. B.; DeNeve, B. A.; Weston, A. *Corrosion* **1991**, *47*, 55.
(5) Schoonen, M. A. A.; Fisher, N. S.; Wente, M. *Geochim. Cosmochim. Acta* **1992**, *56*, 1801.
(6) Eggleston, C. M.; Ehrhardt, J. J.; Stumm, W. *Am. Mineral.* **1996**, *81*, 1036.
(7) Moses, C. O.; Nordstrom, D. K.; Herman, J. S.; Mills, A. L. *Geochim. Cosmochim. Acta* **1987**, *51*, 1561.
(8) Moses, C. O.; Herman, J. S. *Geochim. Cosmochim. Acta* **1991**, *55*, 471.
(9) Goldhaber, M. B. *Am. J. Sci.* **1983**, *283*, 193.
(10) Luther III, G. W. *Geochim. Cosmochim. Acta* **1987**, *51*, 3193.
(11) Luther III, G. W. In *Aquatic Chemical Kinetics*; Stumm, W., Ed.; John Wiley & Sons: New York, 1990; pp 173−198.
(12) Bancroft, G. M.; Hyland, M. M. In *Mineral Water Interface Geochemistry*; Hochella, M. F., White, A. F., Eds.; Mineralogical Society of America: Washington, DC, 1990; Reviews in Mineralogy, Vol. 23, pp 511−558.
(13) Lowson, R. T. *Chem. Rev.* **1982**, *82*, 461.
(14) McKibben, M. A.; Barnes, H. L. *Geochim. Cosmochim. Acta* **1986**, *50*, 1509.
(15) Toniazzo, V. Ph.D. Thesis, Henri Poincaré University, Nancy, 1998.
(16) Zhu, X.; Li, J.; Wadsworth, M. E. *Colloids Surf. A* **1994**, *93*, 201.
(17) Knipe, S. W.; Mycroft, J. R.; Pratt, A. R.; Nesbitt, H. W.; Bancroft, G. M. *Geochim. Cosmochim. Acta* **1995**, *59*, 1079.
(18) Karthe, S.; Szargan, R.; Suoninen, E. *Appl. Surf. Sci.* **1993**, *72*, 157.
(19) Donato, Ph. de; Mustin, C.; Benoit, R.; Erre, R. *Appl. Surf. Sci.* **1993**, *68*, 81.
(20) Mycroft, J. R.; Bancroft, G. M.; McIntyre, N. S.; Lorimer, J. W.; Hill, I. R. *J. Electroanal. Chem.* **1990**, *292*, 139.
(21) Fornasiero, D.; Eijt, V.; Ralston, J. *Colloids Surf. A* **1992**, *62*, 63.
(22) Bebie, J.; Schoonen, M. A. A.; Fuhrmann, M.; Strongin, D. R. *Geochim. Cosmochim. Acta* **1998**, *62*, 633.
(23) Brown, J. R.; Bancroft, G. M.; Fyfe, W. S.; McLean, R. E. N. *Environ. Sci. Technol.* **1979**, *13*, 1142.
(24) Kislinskaya, G. E.; Sheka, I. A.; Kosachek, N. N.; Krasnova, G. M.; Schenk, N. I. *Sov. Prog. Chem.* **1981**, *47*, 92.
(25) Schindler, P. W.; Stumm, W. In *Aquatic Surface Chemistry*; Stumm, W., Ed.; John Wiley & Sons: New York, 1987; pp 83−110.
(26) Stumm, W. *Chemistry of the Solid-Water Interface*; John Wiley & Sons: New York, 1992.
(27) Buckley, A. M.; Woods, R. *Appl. Surf. Sci.* **1987**, *27*, 437.
(28) Mielczarski, J. A.; Cases, J. M.; Alnot, M.; Ehrhardt, J. J. *Langmuir* **1996**, *12*, 2519.
(29) Scofield, J. H. *J. Electron. Spectrosc. Relat. Phenom.* **1976**, *8*, 129.
(30) Seah, M. P.; Dench, W. A. *Surf. Interface Anal.* **1979**, *1*, 2.
(31) Carlson, T. A. *Photoelectron and Auger Spectroscopy*; Plenum Press: New York, 1975.
(32) Pratt, A. R.; Nesbitt, H. W.; Muir, I. J. *Geochim. Cosmochim. Acta* **1994**, *58*, 5147.
(33) Parks, G. A. *Chem. Rev.* **1965**, *65*, 177.
(34) Stumm, W.; Lee, G. F. *Ind. Eng. Chem.* **1961**, *53*, 143.
(35) Meng, X.; Letterman, R. D. *Environ. Sci. Technol.* **1993**, *27*, 970.
(36) Meng, X.; Letterman, R. D. *Environ. Sci. Technol.* **1993**, *27*, 1924.
(37) Nesbitt, H. W.; Muir, I. J. *Geochim. Cosmochim. Acta* **1994**, *58*, 4667.
(38) Mills, P.; Sullivan, J. L. *J. Phys. D: Appl. Phys.* **1983**, *16*, 723.
(39) Harvey, D. T.; Linton, R. W. *Anal. Chem.* **1981**, *53*, 1648.
(40) Ferris, F. G.; Tazaki, K.; Fyfe, W. S. *Chem. Geol.* **1989**, *74*, 321.
(41) Scheidegger, A.; Borkovec, M.; Sticher, H. *Geoderma* **1993**, *58*, 43.
(42) Van der Heide, H.; Hemmel, R.; Van Bruggen, C. F.; Haas, C. *J. Solid State Chem.* **1980**, *33*, 17.
(43) Wagner, C. D.; Riggs, W. M.; Davis, L. E.; Moulder, J. F.; Muilenberg, G. E. *Handbook of X-ray Photoelectron Spectroscopy*; Perkin-Elmer Corporation, 1979.
(44) Hyland, M. M.; Bancroft, G. M. *Geochim. Cosmochim. Acta* **1990**, *54*, 117.
(45) Jones, C. F.; Lecount, S.; Smart, R. St. C.; White, T. *Appl. Surf. Sci.* **1992**, *55*, 65.

Received for review March 4, 1998. Revised manuscript received June 1, 1998. Accepted June 15, 1998.

ES980213C